

Lab on a Chip

Accepted Manuscript



This is an *Accepted Manuscript*, which has been through the Royal Society of Chemistry peer review process and has been accepted for publication.

Accepted Manuscripts are published online shortly after acceptance, before technical editing, formatting and proof reading. Using this free service, authors can make their results available to the community, in citable form, before we publish the edited article. We will replace this *Accepted Manuscript* with the edited and formatted *Advance Article* as soon as it is available.

You can find more information about *Accepted Manuscripts* in the [Information for Authors](#).

Please note that technical editing may introduce minor changes to the text and/or graphics, which may alter content. The journal's standard [Terms & Conditions](#) and the [Ethical guidelines](#) still apply. In no event shall the Royal Society of Chemistry be held responsible for any errors or omissions in this *Accepted Manuscript* or any consequences arising from the use of any information it contains.

PDMS Nanocomposites for Heat Transfer Enhancement in Microfluidic Platforms

Pyshar Yi,^{*a} Robiatun A. Awang,^a Wayne S. T. Rowe,^a Kourosh Kalantar-zadeh,^{*a} and
Khashayar Khoshmanesh^{*a}

^a RMIT University, School of Electrical and Computer Engineering, Melbourne,
Victoria 3001, Australia

E-mail: pyshar.yi@gmail.com

kourosh.kalantar@rmit.edu.au

khashayar.khoshmanesh@rmit.edu.au

Abstract

Increasing the thermal conductivity of PDMS (polydimethylsiloxane) based microfluidics is an important issue for the thermal management of hot spots produced by embedding electronic circuits in such systems. This paper presents a solution for enhancing the thermal conductivity of such PDMS based microfluidics by introducing thermally conductive alumina (Al_2O_3) nanoparticles, forming PDMS/ Al_2O_3 nanocomposites. The materials are fully characterized for different concentrations of Al_2O_3 in PDMS for experiments which are conducted at different flow rates. Our results suggest that incorporation of Al_2O_3 nanoparticles at 10% *w/w* in the PDMS based nanocomposite significantly enhances the heat conduction from hot spots by enhancing the thermal conductivity, while maintaining the flexibility and decreasing the specific heat capacity of the developed materials. This proof-of-concept study offers potential for a practical solution for the cooling of future embedded electronic systems.

Keywords: cooling; heat capacity; heat transfer; microfluidics; thermal conductivity

Introduction

Thermal management in microfluidics is an important challenge. Polymers such as PDMS (polydimethylsiloxane) which are commonly used for the development of microfluidics have small thermal conductivities. As a result, they do not allow the efficient exchange of heat between the localized hot spots and the flowing liquid or the surrounding environment. For many applications such an inefficient heat exchange is not favorable, especially for embedded electronic components (in the form of an integrated circuit (IC)) in microfluidics, which produce significant hot spots that need to be cooled.

Over the past few decades, the revolution in electronics has resulted in the packing of an extraordinary number of transistors within IC chips. Hence, the management of heat generation and large non-uniformities in heat dissipation has emerged as major challenges¹⁻³. Hot spots produce a non-uniform heat flux and increase the chip junction maximum temperature, which in turn reduce the reliability and performance of the embedded electronic devices^{4, 5}. For instance, a temperature increase of 10-15 K above the defined IC chip operating temperature can cause a two-times fall in their life time⁶.

Etched silicon or glass has historically been used to fabricate microfluidic devices, using technology derived from microelectronics/photolithography⁷⁻⁹. Silicon has a high thermal conductivity and can be employed to manage the cooling of hot spots. However, photolithography and etching technologies are expensive for producing high aspect ratio structures used in cooling. Difficulties also arise in bonding or embedding any small devices within their inelastic structures, and their sealing processes require high temperatures¹⁰⁻¹³.

PDMS is a transparent silicone elastomer which has contributed to technology advancements in microfluidics^{2, 10, 13, 14} due to its good stability over a wide range of temperatures, chemical and electrical resistivity, as well as mechanical flexibility after curing^{15, 16}. Despite the advantageous properties of PDMS, it has a poor thermal conductivity of $0.15 \text{ W m}^{-1} \text{ K}^{-1}$ ¹⁷, which is not an ideal material for cooling microfluidic systems.

The incorporation of thermally conductive materials including carbon nanotubes, graphene and metal oxides such as alumina (Al_2O_3) into PDMS have been suggested to enhance the thermal properties of the resulting composites even at very low concentrations¹⁸⁻²³. The challenges of nanocompositing are relevant to obtaining homogenous distributions of the particles within the polymer matrix, compatibility between the nanofillers and the polymer, and assuring that the composite still holds the key properties of PDMS even after nanocompositing. These properties include flexibility and the possibility of thermal curing. Despite the fact that such nanocomposite materials have been used for forming conductive flexible electrodes based on PDMS, they have never been used as the main building blocks of microfluidics²⁴. When used in microfluidics, a key issue which has not been fully addressed is to investigate the thermal properties of the nanocomposites. For many applications, it is desirable to increase the thermal conductivity as much as possible to allow cooling and heating of the liquid and the other components of the microfluidic system as quickly and efficiently as possible.

In this work, we introduce a method to enhance the thermal conductivity of the PDMS matrix for a better heat exchange in microfluidic channels; by mixing it with thermally conductive nanoparticles of Al_2O_3 (a multi-walled-carbon nanotube (MWCNT) composite is also included for comparison). The obtained nanocomposites are fully characterized to reveal their flexibility, thermal properties and nanoparticle homogeneity within the polymeric matrix. Experimental measurements and numerical simulations are presented to fully understand the thermal performance of microfluidic systems made from the developed nanocomposite. This study provides a proof-of-concept, which can offer a practical solution for the cooling of future microelectronics technologies using polymer based microfluidics.

Experimental section

Microfluidic device

To investigate the impact of the increased thermal conductivity of the PDMS/Al₂O₃ nanocomposite on the thermal performance of a microchip, we use a simple microfluidic platform, as shown in Fig. 1. The microfluidic platform consists of a PDMS or PDMS/Al₂O₃ nanocomposite which accommodates a rectangular microchannel with dimensions of 1000 μm × 260 μm (width × height) and 45 mm length that is assembled on a 100 μm thick glass substrate. This substrate thickness is chosen to allow minimal dispersion of heat within the glass base, so the infrared measurements become an accurate depiction of the temperature in the microfluidic channel. A small cylindrical heater with dimensions of 5 mm × 1 mm (diameter × height) is integrated into the PDMS or PDMS/Al₂O₃ nanocomposites to generate heat during the thermal measurements.

Fabrication process

The microchannel is fabricated from PDMS, and PDMS/Al₂O₃ (and for comparison PDMS/MWCNT) nanocomposites using soft photolithography techniques². An SU8-3050 (Microchem, USA) layer is spin coated three times at 1000 rpm on a 3-inch diameter silicon wafer to produce a 260 μm thickness layer. The sample is then exposed to UV light source using an MA6 mask aligner for 3 min with an interval of 1 min between each exposure, and developed in SU-8 developer for 40 min to realize the desired patterns on the master.

The MWCNT (thermal conductivity: ~3,000 W m⁻¹ K⁻¹²⁵, dimensions: 13-18 nm outer diameter and 3-30 μm length) and Al₂O₃ nanoparticles (thermal conductivity: ~40 W m⁻¹ K⁻¹²⁶, average dimension < 50 nm) are purchased from Sigma-Aldrich, Australia.

In order to fabricate the PDMS/Al₂O₃ nanocomposite, the nanoparticles should be thoroughly mixed with PDMS to achieve a homogeneous and uniformly distributed polymer matrix. The procedure begins by adding the desired weight percentage of Al₂O₃ nanoparticles

into the PDMS matrix and manually stirring for 10 min, followed by sonication in an ultrasonic bath (Unisonics, Australia) for a further 20 min. The PDMS curing/crosslinking agent (Sylgard 184, Dow Corning) is added to the mixture to form a 10:1 ratio. The sample is stirred manually for 10 min, and then degassed for 30 min in order to remove the trapped air bubbles using a vacuum oven. The PDMS/ Al_2O_3 nanocomposite is poured onto the master to reach a height of ~ 2 mm and cured on a hot plate with a temperature of 70°C for 7 min.

Next, a small heater made by winding a Eureka wire ($2.2 \Omega/\text{foot}$) around a 5 mm diameter ceramic ring is integrated into the PDMS or PDMS nanocomposite block. The heater is inserted 1 mm away from the side wall of the microchannel. The rest of the PDMS or PDMS nanocomposite mixture is poured into the device to cover the heater and reach the overall height of the PDMS or PDMS nanocomposite block to 6 mm. The device is cured for 20 min on the 70°C hot plate. The substrate is allowed to cool down for 5 min. Then, the PDMS/ Al_2O_3 block of $60 \times 20 \times 6$ mm (length \times width \times height) is carefully peeled from the master. The mixes are all thermally curable for all Al_2O_3 nanoparticles concentrations presented in this paper. The fabrication process is conducted in a class 1000 cleanroom.

The PDMS or PDMS nanocomposite block is integrated onto a glass slide (Menzel-Glaser, USA) of $60 \times 20 \times 0.1$ mm (length \times width \times height). The glass thickness of $100 \mu\text{m}$ is chosen to reduce the temperature drop through the thickness of the glass such that the temperatures measured by the infrared camera can be as close as possible to the temperature of liquid inside the microchannel. Tygon® microtubes with an internal diameter of $400 \mu\text{m}$ are placed into the holes punched in the PDMS block to interface with the sample bottle and the syringe pump. The fabrication process is repeated with different concentrations of PDMS/ Al_2O_3 nanocomposites. The process of fabricating PDMS/MWCNT nanocomposites is very similar.

Apparatus

Fig. 1 shows the experimental setup of the microfluidic system. A syringe pump (Harvard PHD 2000) is used for providing the flow through the microchannel. The syringe pump is operated in refill mode to supply a suction within the microchannel in order to prevent leakage and generation of bubbles within the microchannel. The heater is energized *via* a DC power supply (Gw Instek, GPS-X303 series, Taiwan). An infrared camera (FLIR Systems, ThermoVision A320, Sweden) is used for measuring the temperature across the external surface of the glass substrate, which forms the bottom surface of the microchannel.

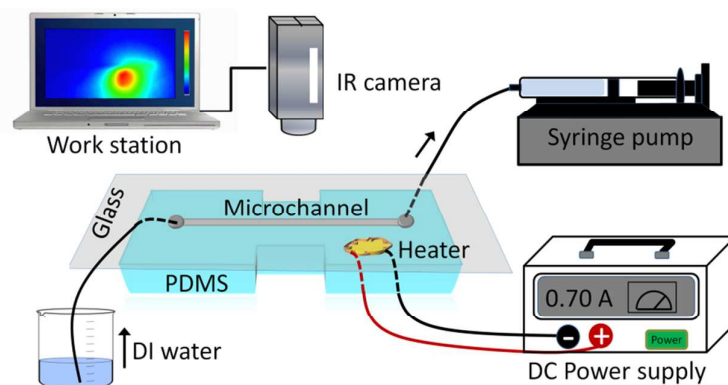


Fig. 1 Experimental setup for thermal measurements of a microfluidic platform with a flow of dionized water.

Results

Homogeneity and roughness of PDMS/ Al_2O_3 nanocomposites

Scanning electron microscope (SEM) imaging of 2 and 10% *w/w* PDMS/ Al_2O_3 nanocomposites (Fig. 2(a)) reveal the existence of Al_2O_3 nanoparticles randomly distributed within the PDMS matrix. The roughness of the composites is investigated by atomic force microscopy (AFM) probing. This reveals that the roughness of the nanocomposites increases to ± 50 and ± 400 nm region values, respectively, for the 2% and 10% *w/w* PDMS/ Al_2O_3 nanocomposites (Fig. 2(b)). It appears that at 10% *w/w* concentration, large islands of Al_2O_3 are formed as a result of some agglomeration of the nanoparticles, while they are much better dispersed at 2% *w/w*. The homogeneity and roughness of PDMS/ Al_2O_3 nanocomposites can be further improved by using a shaker to mix the Al_2O_3 nanoparticles with PDMS matrix, as explained in Supporting Information 1.

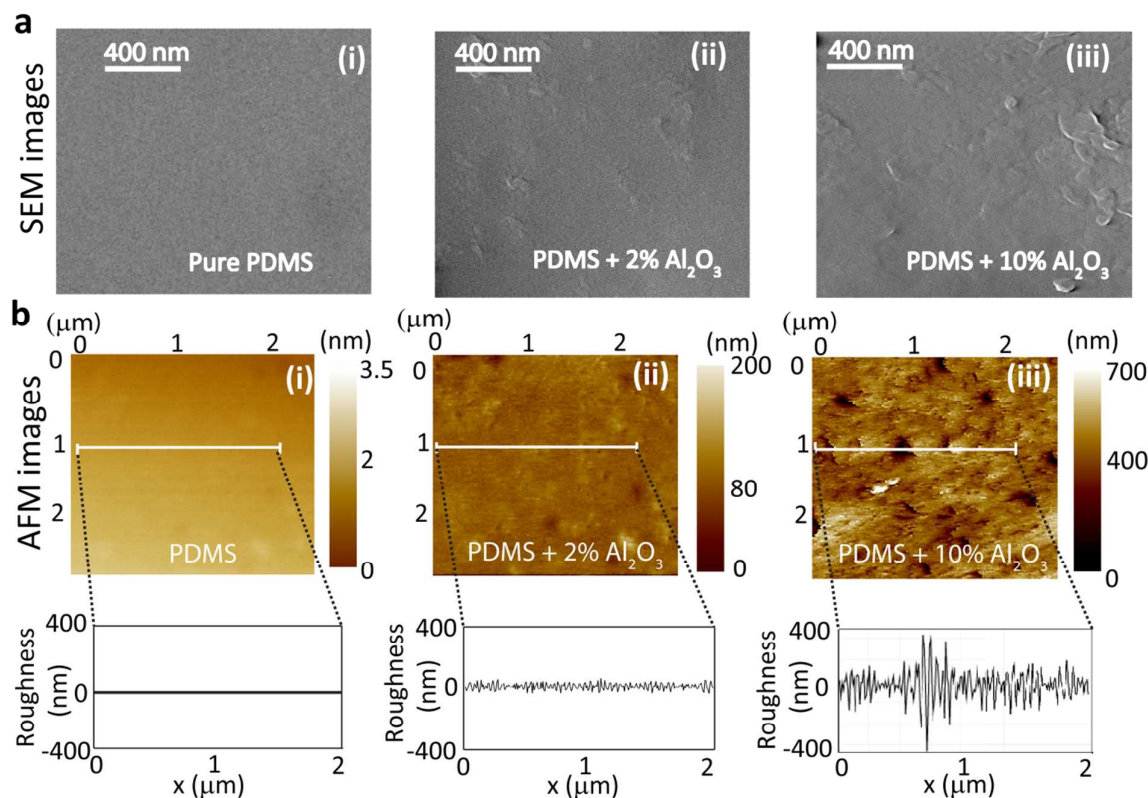


Fig. 2 (a) SEM images of various concentrations of PDMS/ Al_2O_3 nanocomposites at: (i) 0, (ii) 2 and (iii) 10% *w/w*. (b) AFM images taken at: (i) 0, (ii) 2 and (iii) 10% *w/w* PDMS/ Al_2O_3 nanocomposites.

Thermal conductivity and specific heat capacity of PDMS/Al₂O₃ nanocomposites

Fig. 3(a) shows the thermal conductivity and specific heat capacity of PDMS/Al₂O₃ nanocomposites in various concentrations of 0 to 10% *w/w*. As previously presented, the thermal conductivity of pure PDMS is $\sim 0.15 \text{ W m}^{-1} \text{ K}^{-1}$, while it is $\sim 40 \text{ W m}^{-1} \text{ K}^{-1}$ for Al₂O₃. Intuitively, by increasing the concentration of the Al₂O₃ nanoparticles the thermal conductivity of the nanocomposite should also increase. The thermal conductivities of pure PDMS and PDMS/Al₂O₃ nanocomposites are obtained by measuring the temperature drop along cylindrical-shaped structures insulated within in a blue plastic tube (PUN tubing, FESTO), as detailed in Supporting Information 2. Our experiments indicate that the thermal conductivity of PDMS/Al₂O₃ nanocomposite increases from $0.152 \text{ W m}^{-1} \text{ K}^{-1}$ for that of pure PDMS to $0.294 \text{ W m}^{-1} \text{ K}^{-1}$ for the 2% *w/w* nanocomposite. Mixing Al₂O₃ nanoparticles exceeding 5% *w/w*, the thermal conductivity of the nanocomposites become saturated at a value of $\sim 0.35 \text{ W m}^{-1} \text{ K}^{-1}$, and can be expressed by an exponential equation presented in Fig. 3(a). The existence of discrete islands of highly thermally conductive nanoparticles isolated by low conductive PDMS regions that was seen by the AFM profiles (Fig 2(b)) explains the saturation of the composites' thermal conductivity at high concentrations of nanoparticles. Our measurements indicate that the thermal conductivity of the nanocomposite is also affected by the size of Al₂O₃ nanoparticles. For example, using larger Al₂O₃ nanoparticles (with an average dimension of $< 400 \text{ nm}$) the thermal conductivity of the nanocomposite is reduced by $\sim 10\%$, as presented in Supporting Information 3.

The thermal conductivity of PDMS/MWCNT nanocomposite is also shown in Fig. S4 for comparison. A similar trend can be observed for the PDMS/MWCNT nanocomposite. However, the superior thermal conductivity of MWCNTs ($\sim 3,000 \text{ W m}^{-1} \text{ K}^{-1}$) result in a thermal conductivity of $\sim 1.25 \text{ W m}^{-1} \text{ K}^{-1}$, which is almost 4 times larger than that of PDMS/Al₂O₃ nanocomposite of the same concentration and still has not saturated at a concentration of 10% *w/w*. Despite a better thermal performance, the health hazards posed by

MWCNT^{27, 28} prohibited us from further using them in the rest of our work. Another issue regarding nanocomposites of the MWCNT is that they become highly electrically conductive at above ~5% w/w, which is not favorable in many microfluidic systems.

The specific heat capacity of PDMS or PDMS/Al₂O₃ nanocomposites is also obtained by measuring the transient temperature drop of cubic structures and applying the lumped capacity method, as detailed in Supporting Information 5. In contrast to the thermal conductivity, the specific heat capacity of PDMS/Al₂O₃ nanocomposite is seen to exponentially decrease with an increase of Al₂O₃ nanoparticles (Fig. 3(a)). The heat capacity of pure PDMS is 1.38 KJ kg⁻¹ K⁻¹ which reduces to 1.29 KJ kg⁻¹ K⁻¹ by the incorporation of 10% w/w Al₂O₃ nanoparticles.

Elasticity of PDMS/Al₂O₃ nanocomposites

Next, we measure the elasticity (E) of pure PDMS and PDMS/Al₂O₃ nanocomposites using a Universal Testing Machine (UTM; WL 2100; Instron, Norwood, MA) according to the KS M 6518 test method²⁹, as detailed in Supporting Information 6. The average elasticity of the specimens based on 5 times repetition is 2.47, 2.23 and 1.94 MPa for the pure PDMS, 2% and 10% w/w PDMS/Al₂O₃ nanocomposites, respectively (Fig. 3(b)). The elasticity of the nanocomposite drops by increasing the Al₂O₃ concentration. We hypothesize that this is due to the disruption of polymeric chains of the PDMS after the incorporation of Al₂O₃ nanoparticles. To verify this, Raman spectroscopy is conducted.

Raman spectroscopy of PDMS/Al₂O₃ nanocomposites

Raman spectroscopy is employed to identify the changes in the chemical structures of the PDMS after the addition of Al₂O₃ nanoparticles. We focus a monochromatic laser beam with a wavelength of 785 nm onto the surface of the samples and collect the Raman signals using a PerkinElmer[®] RamanStation[™] 400F machine, USA. The spectra are all normalized against

the Raman shift peak at 2964 cm^{-1} (CH_3 asymmetric stretching), as shown in Fig. 3(c). Compared to pure PDMS, the major peak at 2904 cm^{-1} , which corresponds to CH_3 symmetric stretching, decreases by 12% and 17% for the 2% and 10% w/w Al_2O_3 nanocomposites, respectively. This means that the addition of Al_2O_3 increases the disorder of the PDMS polymeric chains. While such an increase in disorder does not affect the asymmetric stretching of CH_3 , it dampens the symmetric stretching of CH_3 component, which are placed out of phase from one another. However, Raman shift peaks between 600 to 900 cm^{-1} are slightly increased by adding Al_2O_3 nanoparticles as Al_2O_3 has two broad peaks at 710 and 860 cm^{-1} ³⁰.

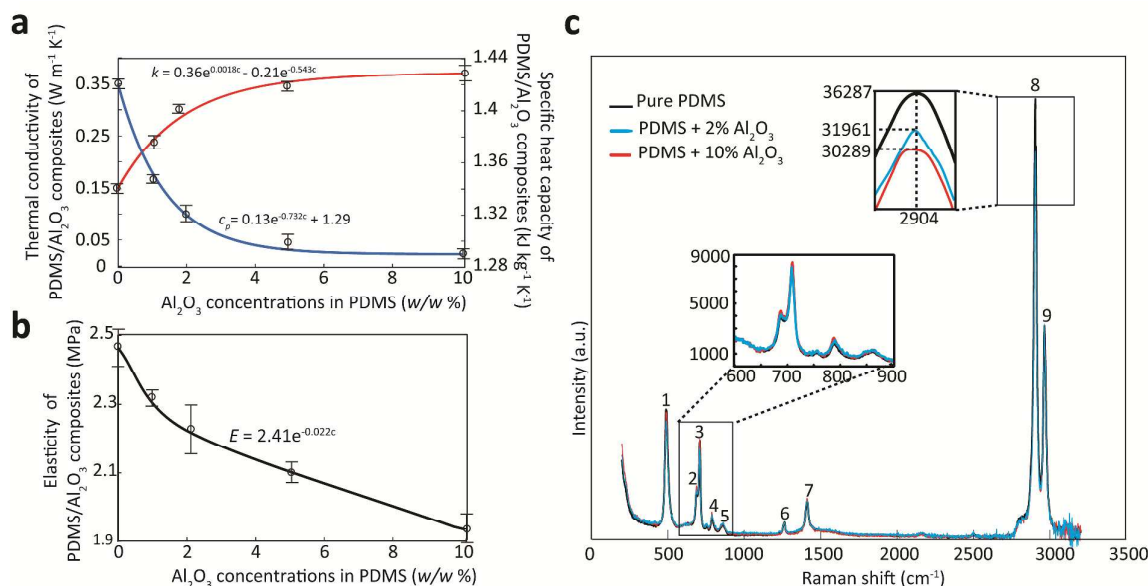


Fig. 3 Thermal, structural and chemical characterization of pure PDMS and PDMS/ Al_2O_3 nanocomposites: (a) Thermal conductivity and specific heat capacity, (b) elasticity, and (c) Raman spectra of pure PDMS and PDMS/ Al_2O_3 nanocomposites. The number at the vibrational peaks represent (1) Si-O-Si symmetric stretching (488 cm^{-1}), (2) Si- CH_3 symmetric rocking (688 cm^{-1}), (3) Si-C symmetric stretching (708 cm^{-1}), (4) CH_3 asymmetric rocking + Si-C asymmetric stretching (788 cm^{-1}), (5) CH_3 symmetric rocking (862 cm^{-1}), (6) CH_3 symmetric bending (1264 cm^{-1}), (7) CH_3 asymmetric bending (1412 cm^{-1}), (8) CH_3 symmetric stretching (2904 cm^{-1}) and (9) CH_3 asymmetric stretching (2964 cm^{-1}). The insets show the close-up images.

Thermal characterization of PDMS/Al₂O₃ nanocomposites

To create localized hot spots within the microfluidic system, the heater is energized with a current of 0.7 A and a voltage of 0.4 V. Deionized water is drawn through the microchannel at the desired flow rates using a syringe pump. The inlet temperature follows the ambient temperature and is measured as 298 ± 0.3 K during the experiments. We obtain thermal images from the view of the 100 μm thick glass substrate using an infrared camera, as described in our previous work²⁶. The measurements are conducted approximately 15-20 min after the operation of the system to ensure it has reached its steady state conditions.

Fig. 4(a-c) show the top-view of the microfluidic platforms for the cases of (i) pure PDMS, (ii) PDMS with 2% w/w Al₂O₃ and (iii) PDMS with 10% w/w Al₂O₃ nanoparticles. While the pure PDMS is transparent the addition of Al₂O₃ nanoparticles makes it rather milky, even at a low concentration of 2% w/w. Despite this, the nanocomposites are still soft and flexible (see Fig. 2(b)). Fig. 4(d-f) represent the obtained temperature contours at the glass substrate for the cases (i-iii) at the flow rate of 40 $\mu\text{l min}^{-1}$.

In case (i), a hot spot with a maximum temperature of 326 K is formed at the surface of the glass (Fig. 4(d)). The heat propagates through PDMS *via* conduction, as evidenced by the symmetric distribution of temperature contours around the hot spot. However, the low thermal conductivity of the pure PDMS ($0.152 \text{ W m}^{-1} \text{ K}^{-1}$, Fig. 2(a) leads to sharp temperature gradients across the surface. Approaching the microchannel, the temperature contours are stretched to the right due to convection. Similar trends can be observed for cases (ii) and (iii). However, the increased thermal conductivity of the PDMS/Al₂O₃ nanocomposites ($0.294 \text{ W m}^{-1} \text{ K}^{-1}$ for case (ii) and $0.364 \text{ W m}^{-1} \text{ K}^{-1}$ for case (iii)) facilitates the propagation of heat through the matrix, which in turn reduces the temperature of the hot spot to 322 and 318 K, respectively.

To further characterize the impact of the increased thermal conductivity of the matrix, we plot the variations of temperature along three arbitrary lines parallel to the microchannel (Fig. 4(g-i)). This includes line *A* which lies along the middle of the hot spot, line *B* which lies along the hot side wall of the microchannel and line *C* which lies along the cold side wall of the microchannel. The temperature varies along these three lines with a similar trend. The temperature at the far left of the lines (inlet of the microchannel) is the same as the ambient temperature, and increases gradually until reaching a peak temperature along the hot spot and then decreases towards the outlet of the microchannel. The temperature peaks observe along these three lines can be considered as the characteristic temperatures of the system, as they show the propagation of heat both within the PDMS matrix and the microchannel, and thus are referred to as $T_{hot\ spot}$, $T_{hot\ wall}$ and $T_{cold\ wall}$ for the lines *A*, *B* and *C*, respectively.

In case (i), the three characteristic temperatures are measured as $T_{hot\ spot} = 326$ K, $T_{hot\ wall} = 317$ K and $T_{cold\ wall} = 308$ K. The addition of 2% w/w Al_2O_3 nanoparticles into the PDMS in case (ii) reduces the temperatures along the lines *A*, *B* and *C*, as evidenced by dropping the three characteristic temperatures to $T_{hot\ spot} = 322$ K, $T_{hot\ wall} = 313$ K and $T_{cold\ wall} = 307$ K. Further increase of Al_2O_3 concentration to 10% w/w in case (iii) leads to further cooling of the system, and reduces the three characteristic temperatures to $T_{hot\ spot} = 318$ K, $T_{hot\ wall} = 307.5$ K and $T_{cold\ wall} = 305.5$ K.

It should be considered that the system operates in a steady state mode, and thus the heat capacity change does not affect its performance. However, in a dynamic mode, the effect of the heat capacity decrease (from $1.38\text{ KJ kg}^{-1}\text{ K}^{-1}$ for pure PDMS to $1.29\text{ KJ kg}^{-1}\text{ K}^{-1}$ for case (iii)) should result in relatively faster temperature changes in the system.

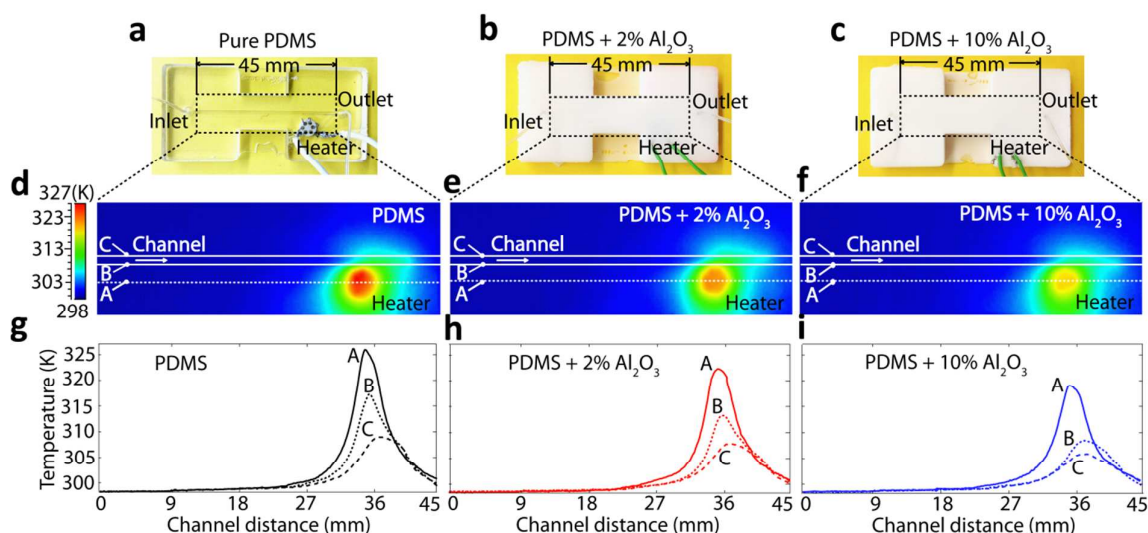


Fig. 4 Analysing the thermal performance of the microfluidic platform following the addition of Al₂O₃ nanoparticles. (a-c) The top-view of the microfluidic platform with 0%, 2% and 10% w/w Al₂O₃ nanoparticles. (d-f) Temperature contours across the bottom surface of the glass substrate for the PDMS nanocomposites with 0%, 2% and 10% w/w Al₂O₃ nanoparticles. (g-i) Temperature variations along three arbitrary lines along the surface of glass substrate for the PDMS nanocomposites with 0%, 2% and 10% w/w Al₂O₃ nanoparticles. Results are obtained when deionized water flow through the microchannel at a rate of 40 $\mu\text{l min}^{-1}$.

Numerical simulations

In addition, a comprehensive set of computational fluid dynamics (CFD) simulations are conducted to explore the variations of temperature at different locations of the system, including its internal cross sections, which cannot be measured using the thermal imaging camera. The simulations are conducted at a flow rate of 40 $\mu\text{l min}^{-1}$, and using PDMS/Al₂O₃ nanocomposites with different Al₂O₃ concentrations of 0, 2 and 10 % w/w (Fig. 5), as detailed in Supporting Information 7.

Fig. 5(a-c) illustrate the simulated temperatures across the bottom surface of the glass substrate, which are in line with the measured temperatures shown in Fig. 4(d-f). The results clearly show the consistent decrease of temperature across the bottom surface following the incorporation of Al₂O₃ nanoparticles into the PDMS matrix, and also depict the different configuration of temperature contours along the two sides of the microchannel due to the

presence of convective heat transfer within the microchannel. Fig. 5(d-f) show the calculated temperature contours across the external surface of PDMS/ Al_2O_3 nanocomposites exposed to air. The results clearly show the improved propagation of heat throughout the system by increasing the concentration of Al_2O_3 nanoparticles. In Fig. 5(d) the maximum temperature of the top and side walls is 311.2 K, however the majority of the surface experiences a temperature of 298 K. In contrast, in Fig. 5(f) while the maximum temperature of the top and side walls drops to 310 K the majority of the surface has a temperature of more than 300 K and thus can exchange heat with the surrounding air by means of free convection. Similar trends can be seen across the different cross sections of the system in Fig. 5(g-i).

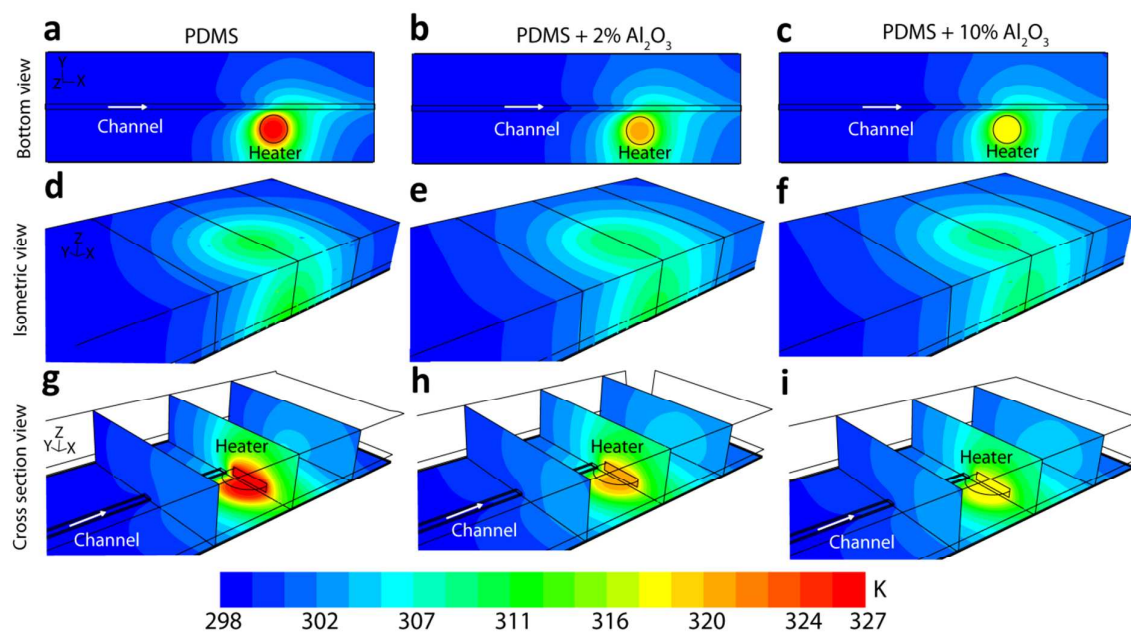


Fig. 5 Temperature contours obtained by CFD simulations for the cases of (i) pure PDMS, (ii) PDMS/ Al_2O_3 nanocomposite with 2% *w/w* of Al_2O_3 nanoparticles and (iii) PDMS/ Al_2O_3 nanocomposite with 10% *w/w* Al_2O_3 nanoparticles. (a-c) Temperature contours across the bottom surface of the glass substrate, (d-f) Temperature contours across the PDMS/ Al_2O_3 nanocomposite surface, (g-i) Temperature contours across three cross sections of the system. Results are obtained by setting the flow rate of deionized water to $40 \mu\text{l min}^{-1}$, the ambient temperature to 298 K and the natural convection coefficient to $10 \text{ W m}^{-1} \text{ K}^{-1}$.

Thermal performance of PDMS/Al₂O₃ nanocomposites under various flow rates

To further understand the thermal performance of the system at different operating conditions, we conduct thermal measurements at different flow rates of 10, 40 and 120 $\mu\text{l min}^{-1}$ using various PDMS/Al₂O₃ nanocomposites with 0, 2 and 10% *w/w* concentrations of Al₂O₃ nanoparticles, which are referred to as cases (i), (ii) and (iii) (Fig. 6). Thermal images are taken similar to those described for the case of 40 $\mu\text{l min}^{-1}$.

Fig. 6(a-c) show the temperature contours across the bottom surface of the glass substrate at a flow rate of 10 $\mu\text{l min}^{-1}$. At such a low flow rate, the heat transfer inside the microchannel is governed by conduction (Péclet number = 0.0018), as evidenced by the symmetric propagation of temperature around the hot spot even after reaching the microchannel. In case (i), a peak temperature of 327 K is measured at the hot spot, which reduces to 323.5 K and 320 K, respectively for cases (ii) and (iii). Fig. 6(d-f) show the temperature contours at the surface of glass substrate at a flow rate of 40 $\mu\text{l min}^{-1}$. At this flow rate, heat transfer inside the microchannel is governed by both conduction and convection (Péclet number = 0.0074), as evidenced by stretching of temperature contours after reaching the microchannel. In case (i), a peak temperature of 326 K is measured at the hot spot, which drops to 322 K and 318 K, respectively for cases (ii) and (iii). Finally, Fig. 6(g-i) show the temperature contours at the surface of the glass substrate at a flow rate of 120 $\mu\text{l min}^{-1}$. At such a high flow rate, heat transfer inside the microchannel is governed by convection (Péclet number = 0.0222), as evidenced by vanishing the green temperature contours after reaching the microchannel. In case (i) a peak temperature of 324 K is measured at the hot spot, which reduces to 320 K and 318 K, respectively for cases (ii) and (iii).

For further comparison, Fig. 6(j) depicts the variation of temperature along a line *A* which passes through the middle of the heater. Interestingly, the microfluidic system with 10% *w/w* Al₂O₃ nanoparticle operating at a low flow rate of 10 $\mu\text{l min}^{-1}$ is 4 K colder than the

system with pure PDMS at a high flow rate of $120 \mu\text{l min}^{-1}$. This is significant as the incorporation of PDMS/ Al_2O_3 nanocomposite removes the need of high flow rate for cooling of microplatforms (see Fig. S7 for comparing the variation of temperature along arbitrary lines *B* and *C* at different flow rates).

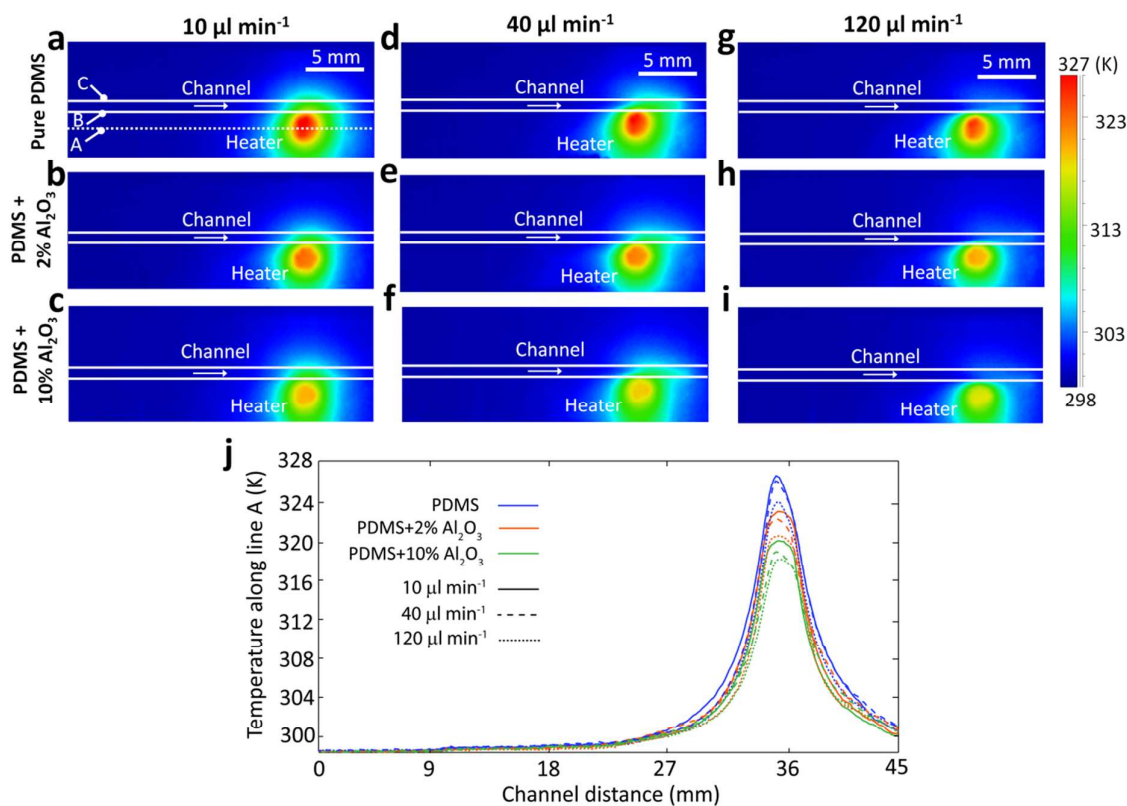


Fig. 6 Temperature contours obtained across the bottom surface of the glass substrate for the PDMS nanocomposites with 0%, 2% and 10% *w/w* Al_2O_3 nanoparticles at different flow rates of: (a-c) $10 \mu\text{l min}^{-1}$, (d-f) $40 \mu\text{l min}^{-1}$ and (g-i) $120 \mu\text{l min}^{-1}$ and (j) Variation of temperatures along a line *A* (hot spot) for all PDMS nanocomposites cases (0, 2 and 10% *w/w*) and flow rates (10, 40 and $120 \mu\text{l min}^{-1}$).

Conclusion

In summary, we fully investigated the properties of PDMS/Al₂O₃ nanocomposites in terms of their structural and thermal properties. After mixing the Al₂O₃ nanoparticles with the PDMS base and adding the curing agent the mixture was curable even at 10% *w/w* nanoparticles concentrations. After thermal curing, the resulting nanocomposite also retained its elasticity. Consequently, we demonstrated the thermal performance of simple microfluidic platforms, using the developed PDMS/Al₂O₃ nanocomposites with improved thermal conductivity. Our measurements indicated that the addition of Al₂O₃ nanoparticles into the PDMS matrix enhanced the thermal conductivity of the matrix from 0.152 W m⁻¹ K⁻¹ for the case of pure PDMS to 0.294 and 0.364 W m⁻¹ K⁻¹, for the cases of PDMS/Al₂O₃ nanocomposites with 2 and 10% *w/w* concentrations of nanoparticles, respectively. This improved the heat transfer within the system and reduced the temperature of the hot spot from 326 K for the case of pure PDMS to 322 K (4 K reduction) and 318 K (8 K reduction), for the cases of 2% and 10% *w/w* Al₂O₃ nanocomposites, respectively, when deionised water flows through the microchannel at a rate of 40 μl min⁻¹. Similar trends were observed at the flow rates of 10 and 120 μl min⁻¹. The experimental techniques reported here should be readily applicable to other nanocomposite materials for investigating their thermal performance. This proof-of-concept study reveals that nanocomposites made of highly thermally conductive nanoparticles, can contribute to development of advanced materials with superior thermal properties for cooling of future microelectronics.

Acknowledgement

K. Khoshmanesh acknowledges the Australian Research Council for funding under Discovery Early Career Researcher Award (DECRA) scheme (DE-120101402). The authors also acknowledge the facilities, and the technical assistance of the Australian Microscopy & Microanalysis Research Facility at the RMIT Microscopy and Microanalysis Facility of RMIT University.

1. P. Ball, *Nature*, 2012, **492**, 174-176.
2. P. Yi, K. Khoshmanesh, J. L. Campbell, P. Coughlan, K. Ghorbani and K. Kalantar-zadeh, *Lab on a Chip*, 2014, **14**, 1604-1613.
3. C. Green, A. G. Fedorov and Y. K. Joshi, *Journal of Electronic Packaging*, 2009, **131**, DOI: 10.1115/1.3104029.
4. S. Im, K. Banerjee and I. IEEE, *Full chip thermal analysis of planar (2-D) and vertically integrated (3-D) high performance ICs*, 2000, 727-730.
5. E. S. Cho, J. M. Koo, L. Jiang, R. S. Prasher, M. S. Kim, J. G. Santiago, T. W. Kenny, K. E. Goodson and I. IEEE, in *Nineteenth Annual IEEE Semiconductor Thermal Measurement and Management Symposium*, 2003, 242-246.
6. V. R. V, W. A and L. and V, *Intel Technologies Journal*, 2000, **Q3**, 1.
7. J. C. McDonald, D. C. Duffy, J. R. Anderson, D. T. Chiu, H. K. Wu, O. J. A. Schueller and G. M. Whitesides, *Electrophoresis*, 2000, **21**, 27-40.
8. S. R. Liu, Y. N. Shi, W. W. Ja and R. A. Mathies, *Analytical Chemistry*, 1999, **71**, 566-573.
9. A. Manz, N. Graber and H. M. Widmer, *Sensors and Actuators B-Chemical*, 1990, **1**, 244-248.
10. J. Kuncova-Kallio, P. J. Kallio and Ieee, *2006 28th Annual International Conference of the IEEE Engineering in Medicine and Biology Society, Vols 1-15*, 2006, 2688-2691.
11. Q. Xiang, G. Q. Hu, Y. L. Gao and D. Q. Li, *Biosensors & Bioelectronics*, 2006, **21**, 2006-2009.
12. C. H. Wang and G. B. Lee, *Biosensors & Bioelectronics*, 2005, **21**, 419-425.
13. P. Yi, K. Khoshmanesh, A. F. Chrimes, J. L. Campbell, K. Ghorbani, S. Nahavandi, G. Rosengarten and K. Kalantar-zadeh, *Advanced Energy Materials*, 2014, **4**, DOI: 10.1002/aenm.201300537.
14. E. Berthier, E. W. K. Young and D. Beebe, *Lab on a Chip*, 2012, **12**, 1224-1237.
15. E. K. Sackmann, A. L. Fulton and D. J. Beebe, *Nature*, 2014, **507**, 181-189.
16. X. Gong and W. Wen, *Biomechanics*, 2009, **3**.
17. J. B. Wu, W. B. Cao, W. J. Wen, D. C. Chang and P. Sheng, *Biomechanics*, 2009, **3**, DOI: 10.1063/1.3058587.
18. K. T. S. Kong, M. Mariatti, A. A. Rashid and J. J. C. Busfield, *Composites Part B-Engineering*, 2014, **58**, 457-462.
19. M. Wang, H. Y. Chen, W. Lin, Z. Li, Q. Li, M. H. Chen, F. C. Meng, Y. J. Xing, Y. G. Yao, C. P. Wong and Q. W. Li, *Acs Applied Materials & Interfaces*, 2014, **6**, 539-544.

20. J. Yu and G. Cennini, *Thermal Investigations of ICs and Systems (THERMINIC), 2013 19th International Workshop on*, 2013, 176-180.
21. W. Y. Zhou, S. H. Qi, C. C. Tu and H. Z. Zhao, *Journal of Applied Polymer Science*, 2007, **104**, 2478-2483.
22. J. Hong, J. Lee, D. Jung and S. E. Shim, *Thermochimica Acta*, 2011, **512**, 34-39.
23. M. B. Bryning, D. E. Milkie, M. F. Islam, J. M. Kikkawa and A. G. Yodh, *Applied Physics Letters*, 2005, **87**, DOI: 10.1063/1.2103398.
24. H. Cong and T. Pan, *Advanced Functional Materials*, 2008, **18**, 1912-1921.
25. P. Kim, L. Shi, A. Majumdar and P. L. McEuen, *Physical Review Letters*, 2001, **87**, DOI: 10.1103/PhysRevLett.87.215502.
26. P. Yi, A. A. Kayani, A. F. Chrimes, K. Ghorbani, S. Nahavandi, K. Kalantar-zadeh and K. Khoshmanesh, *Lab on a Chip*, **2012**, **12**, 2520-2525.
27. C. W. Lam, J. T. James, R. McCluskey, S. Arepalli and R. L. Hunter, *Critical Reviews in Toxicology*, 2006, **36**, 189-217.
28. K. Aschberger, H. J. Johnston, V. Stone, R. J. Aitken, S. M. Hankin, S. A. K. Peters, C. L. Tran and F. M. Christensen, *Critical Reviews in Toxicology*, 2010, **40**, 759-790.
29. J. Park, S. Yoo, E.-J. Lee, D. Lee, J. Kim and S.-H. Lee, *BioChip Journal*, 2010, **4**, 230-236.
30. S. T. Aruna, V. K. W. Grips and K. S. Rajam, *Journal of Applied Electrochemistry*, 2010, **40**, 2161-2169.

This work introduces a method to enhance the thermal conductivity of PDMS microfluidic platforms through the use of PDMS/ Al_2O_3 nanocomposites.

